Statistical Analysis of the Differential Deep Penetration of Energetic Electrons and Protons Into the Low L Region (L<4)

H. Zhao[1], S. T. Califf[2], R. Goyal[1], X. Li[3], M. Gkioulidou[4], J. W. Manweiler[5], and S. Krantz[1]

1 Department of Physics, Auburn University, Auburn, AL, USA

2 CIRES, University of Colorado Boulder, Boulder, CO, USA

3 LASP, University of Colorado Boulder, Boulder, CO, USA

4 Applied Physics Laboratory, Johns Hopkins University, Laurel, MD, USA

5 Fundamental Technologies, LLC, Lawrence, KS, USA

Abstract

Deep penetration of energetic electrons (10s – 100s of keV) to low L-shells (L<4), as an important source of inner belt electrons, is commonly observed during geomagnetically active times. However, such deep penetration is not observed as frequently for similar energy protons, for which underlying mechanisms are not fully understood. To study their differential deep penetration, we conducted a statistical analysis using phase space densities (PSD) of μ=10–50 MeV/G, K=0.14 $G^{1/2}$Re electrons and protons from multi-year Van Allen Probes observations. The results suggest systematic differences in electron and proton deep penetration: electron PSD enhancements at low L-shells occur more frequently, deeply, and faster than protons. For μ=10–50 MeV/G electrons, the occurrence rate of deep penetration events (defined as daily-averaged PSD enhanced by at least a factor of 2 within a day at L<4) is ~2 – 3 events/month. For protons, only ~1 event/month was observed for μ=10 MeV/G, and much fewer events were identified for μ>20 MeV/G. Leveraging dual-Probe configurations, fast electron deep penetrations at L<4 are revealed: ~70% of electron deep penetration events occurred within ~9 hours; ~8% – 13% occurred even within 3 hours, with lower-μ electrons penetrating faster than higher-μ electrons. These results suggest non-diffusive radial transport as the main mechanism of electron deep penetrations. In comparison, proton deep penetration happens at a slower pace. Statistics also show that the electron PSD radial gradient is much steeper than protons prior to deep penetration events, which can be responsible for these differential behaviors of electron and proton deep penetrations.

Key points:

1. Statistical analysis reveals that energetic electron deep penetration to L<4 occurs more frequently, deeply, and faster than protons;
2. Most electron deep penetrations occurred on a timescale of several hours, indicating non-diffusive radial transport as the main mechanism;
3. Such differential deep penetration of different species can be explained by the steeper PSD radial gradient of electrons than protons.

1. Introduction

Earth's radiation belts are the donut-shaped regions where energetic electrons and protons are geomagnetically trapped in Earth's inner magnetosphere. The equilibrium structure of Earth's radiation belts consists of an outer radiation belt, occupied by electrons with energies from 10s of keV to ~10 MeV, and an inner radiation belt, filled with 10s – 100s of keV electrons and 10s of MeV - GeV protons. The energetic electron fluxes are usually low between the two belts, where the slot region resides. However, deep penetration of energetic electrons into the slot region or even the inner belt frequently happens, especially during geomagnetically active times (e.g., Zhao and Li, 2013; Reeves et al., 2016; Turner et al., 2016; Zhao et al., 2016, 2017; Califf et al., 2017, 2022; Claudepierre et al., 2017; Li et al., 2017; Lejosne et al., 2018; Khoo et al., 2021). Furthermore, such deep penetration of energetic electrons, most often seen in energies of 10s – 100s of keV, is believed to be a major source of inner belt electrons (e.g., Turner et al., 2016). Thus, understanding its characteristics and underlying physical mechanisms is critical in understanding the radiation belt dynamics.

Previous studies have revealed the energy- and L-dependent features of energetic electron deep penetration into the slot region and inner belt. Using 100s of keV electron flux observations from the DEMETER satellite, Zhao and Li (2013) found frequent electron flux enhancements in the slot region and inner belt, and these enhancements often happened faster for lower-energy electrons than higher-energy ones. Using Van Allen Probes observations of keV – MeV electrons, Reeves et al. (2016) showed that the flux enhancements of inner belt and slot region electrons are more frequent at lower energies and also tend to happen at lower L-shells for the lower-energy electrons. After enhancement, the decay of electron flux is consistent with the timescale of plasmaspheric hiss wave scattering (e.g., Ripoll et al., 2016). Further focusing on the sudden electron flux enhancement (flux enhanced by more than one order of magnitude within a day at L<3), Turner et al. (2016) showed that such enhancements frequently happened (~2.5/month at 200 keV), and the number of such events decreases exponentially with increasing energy in 100s of keV range. Analyzing the electron phase space density (PSD) radial profile during multiple events, they also showed that such sudden enhancements are an important source of inner belt electrons.

Various mechanisms have been proposed to explain electron deep penetration to low L-shells. The electric field impulses induced by interplanetary shocks can transport energetic particles earthward to very low L-shells (e.g., Blake et al., 1992; Li et al., 1993). However, such enhancements in the inner belt and slot region require intense shocks that are infrequently observed (e.g., Schiller et al., 2016). Substorm injection is also an important mechanism for energetic particles accessing the inner magnetosphere, but direct injection into L<4 is rare (e.g., Turner et al., 2015). Radial diffusion has long been recognized as a potential mechanism for electron enhancements in the slot region and inner belt (e.g., Lyons and Thorne, 1973; Zhao and Li, 2013). However, it usually happens in a relatively slow manner and thus is insufficient to account for some observed fast injections of 10s – 100s of keV electrons in the low L region

(e.g., Su et al., 2016). Non-diffusive radial transport by DC electric fields is a promising mechanism for energetic electron deep penetration to low L-shells. It can be caused by enhanced large-scale electric fields (e.g., Su et al., 2016; Califf et al., 2017; Zhao et al., 2017) or localized DC electric fields such as Subauroral Polarization Streams (SAPS) electric fields (e.g., Califf et al., 2016, 2022; Zhao et al., 2017; Lejosne et al., 2018).

On the other hand, 10s – 100s of keV protons are essential constituents of Earth's ring current, a toroidal electric current flowing around Earth in response to solar drivers (e.g., Frank et al., 1967; Smith and Hoffman, 1973; Williams, 1981; Krimigis et al., 1985; Daglis et al., 1999; Zhao et al., 2015; Gkioulidou et al., 2016). However, their flux enhancements at low L-shells are less frequent than electrons with similar energies (e.g., Zhao et al., 2016, 2017; Califf et al., 2022). Figure 1 shows the daily-averaged fluxes of (left) electrons and (right) protons of energies from ~50 keV to ~500 keV, using data from the Van Allen Probes from 15 March 2013 to 16 July 2019. The daily-averaged Dst index is shown in the bottom panels. As shown in Figure 1, 10s of keV electrons and protons penetrate to low L-shells relatively often. After their enhancements at low L, proton fluxes decayed very fast, while electron fluxes in the inner belt stayed elevated much longer. For 100s of keV energies, however, significant differences can be observed in the occurrence frequency of electron and proton deep penetrations. 100s of keV electron flux enhancements were often observed at L<3, while 100s of keV proton flux enhancements at L<3 were only observed during intense geomagnetic storms. At low L-shells, protons generally display less dynamic features than electrons of similar energies.

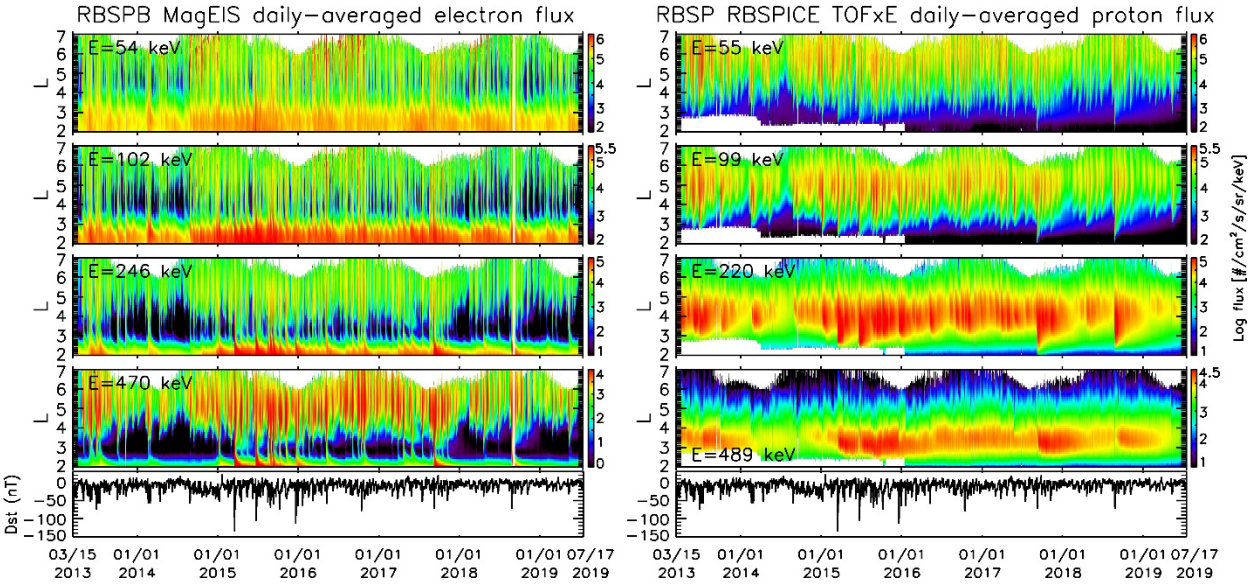

Figure 1. Daily-averaged fluxes of (left) electrons and (right) protons of various energies from 15 March 2013 to 16 July 2019, using data from MagEIS-B and RBSPICE instruments on the Van Allen Probes. The blank areas at L<~2.5 – 3 in proton plots of early years are due to no measurement.

Previous studies have recognized the deep penetration differential behaviors between electrons and protons. However, these systematic differences have never been quantified, and the underlying mechanism causing such differences is still a mystery. While an enhanced convection electric field seems a viable explanation for electron deep penetrations, it can hardly explain the differences between deep penetrations of electrons and protons of similar energies. If the convection electric field is symmetric at dawn and dusk, such as the one predicted by the Volland-Stern electric field model (Volland, 1973; Stern, 1973), protons and electrons with similar energies should penetrate to approximately the same L-shell (e.g., Korth et al., 1999; Lejosne et al., 2018; Califf et al., 2022). On the other hand, the majority of previous studies on the deep penetration of energetic particles focused only on flux enhancements. However, flux variations are subject to the influence of adiabatic effects, which may hinder the identification of underlying physical mechanisms. Thus, in this study, we focus on the electron and proton PSD calculated using pitch-angle-resolved fluxes from Van Allen Probes observations and statistically investigate the differences between electron and proton deep penetrations in terms of the penetration frequency, depth, timescale, and energy dependence. As a result, differential deep penetrations of energetic electrons and protons are quantified, and underlying mechanisms are explored.

2. Data and Analysis

2.1 Phase Space Density of Energetic Electrons and Protons

In this section, we use the pitch-angle-resolved fluxes of energetic electrons from MagEIS instruments (Blake et al., 2013; Claudepierre et al., 2021) and protons from RBSPICE instruments (Mitchell et al., 2013) on the Van Allen Probes (Mauk et al., 2012), from 15 March 2013 to 16 July 2019, to calculate the electron and proton PSD. MagEIS instruments provided differential flux measurements of electrons with energies from ~30 keV to ~4 MeV. RBSPICE instruments TOFxE data are used for proton differential fluxes with energies from ~45 keV to ~600 keV. Observations from both Van Allen Probes were used to provide a better spatiotemporal resolution. Using these pitch-angle-resolved flux data, we calculated the electron and proton PSD as $f = \frac{j}{p^2}$, where j is the differential flux and p is the relativistic momentum. The corresponding adiabatic invariants, μ, K, and L^*, were calculated under the T89D geomagnetic field model (Tsyganenko, 1989) using the Van Allen Probes MagEphem files. In this study, we focus on electrons and protons with μ=10 – 50 MeV/G and K=0.14 $G^{1/2}Re$. These μ and K values roughly correspond to ~50 – 500 keV electrons and ~50 – 700 keV protons at L^*=3 – 4 when Kp=6, and thus are suitable to study the deep penetration of 10s – 100s of keV particles to low L-shells.

Figure 2 shows daily-averaged PSD of electrons and protons with μ=10, 20, 30, and 50 MeV/G and K=0.14 $G^{1/2}Re$, from 15 March 2013 to 16 July 2019, using data from both Van Allen Probes. The differences in electron and proton deep penetrations are even more dramatic in

PSD plots compared to the flux plots. For μ=10 – 50 MeV/G electrons (left panels), deep penetration into L^*<4 and even L^*<3 frequently occurred, causing PSD enhancements of orders of magnitude at low L-shells. After the deep penetration, the electron PSD decreased relatively rapidly in the low L region. For protons, however, such deep penetration occurred much less often than electrons with similar μ and K values. For μ=10 MeV/G protons, deep penetration to L^*=4 occurred relatively often; however, these deep penetrations mostly stopped around L^*~3 and did not reach lower L^*. For μ=20 – 50 MeV/G protons, very few PSD enhancements at L^*<4 can be observed, and PSDs at low L^* are less dynamic than electrons. The energy dependence in electron and proton deep penetrations is also apparent from PSD plots: as μ gets higher, the frequency of deep penetrations becomes lower for both species. On the other hand, both electrons and protons show higher PSDs at higher L-shells in general, which suggests that the source region of these populations at low L-shells is likely located at high L-shells, consistent with the results of electrons shown in Turner et al. (2016). It is also worth noting that the color bars of electron and proton PSDs are different: the radial gradient of electron PSD is commonly much larger than that of proton PSD.

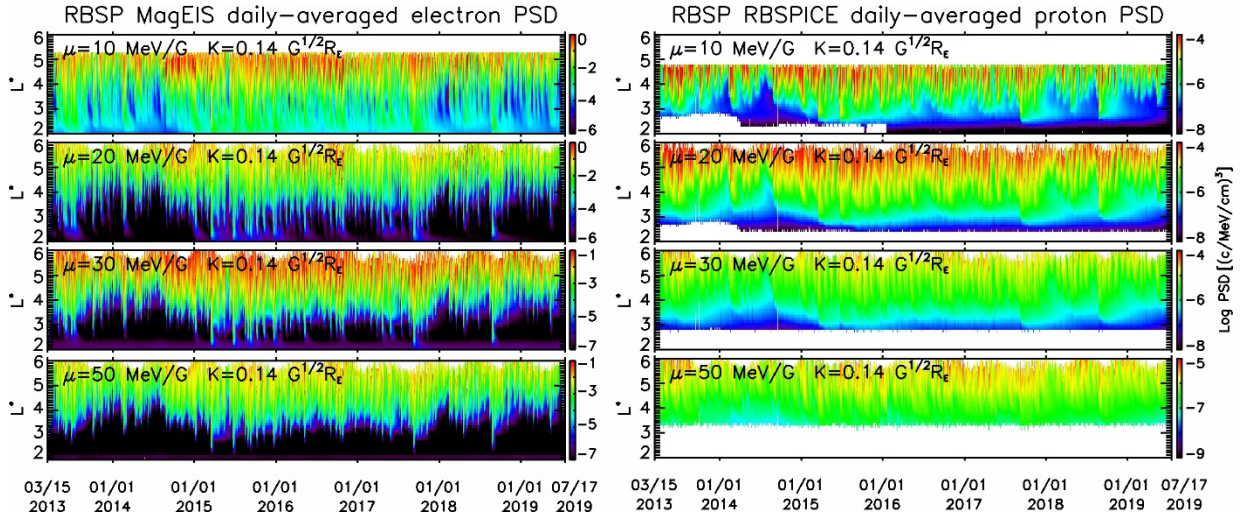

Figure 2. Daily-averaged phase space density of (left) electrons and (right) protons with μ=10, 20, 30, and 50 MeV/G and K=0.14 $G^{1/2}$Re, from 15 March 2013 to 16 July 2019, using data from both Van Allen Probes. The blank areas at low L-shells in μ=20 – 50 MeV/G proton plots are due to the limited energy range of measurements.

2.2 Occurrence Frequency and Depth of Energetic Electron and Proton Deep Penetration Based on the Phase Space Density Data

To quantitatively study the differences between electron and proton deep penetrations, we developed an automatic algorithm to identify such deep penetration events for electrons and protons using their daily-averaged PSD. We define a deep penetration event as the daily-averaged PSD increasing by at least a factor of 2 within a day over ΔL^*≥0.5 at L^*<4. Multiple

enhancements that occur on adjacent days are counted as one single event. Figure 3(a) shows the number of deep penetration events of electrons (in black) and protons (in red) as a function of μ from 15 March 2013 to 16 July 2019. It quantitatively shows both species- and energy-dependent features of these deep penetrations: the number of deep penetration events for electrons is much larger than protons with the same μ and K, and the number of deep penetration events decreases as μ increases for both electrons and protons. About 150 to 250 deep penetration events were observed for μ=10 – 50 MeV/G, K=0.14 $G^{1/2}Re$ electrons over this period, giving an occurrence rate of ~2 – 3 events/month. For μ=10 MeV/G, K=0.14 $G^{1/2}Re$ protons, about 70 events were observed, yielding a ~1 event/month occurrence rate. However, as μ increases, the number of proton deep penetrations drops drastically: very few deep penetration events were identified for μ>20 MeV/G, K=0.14 $G^{1/2}Re$ protons based on our definition. These results demonstrate that electrons penetrate to low L-shells much more frequently than protons of similar energies, and lower energy particles penetrate to low L-shells more easily than higher energy particles.

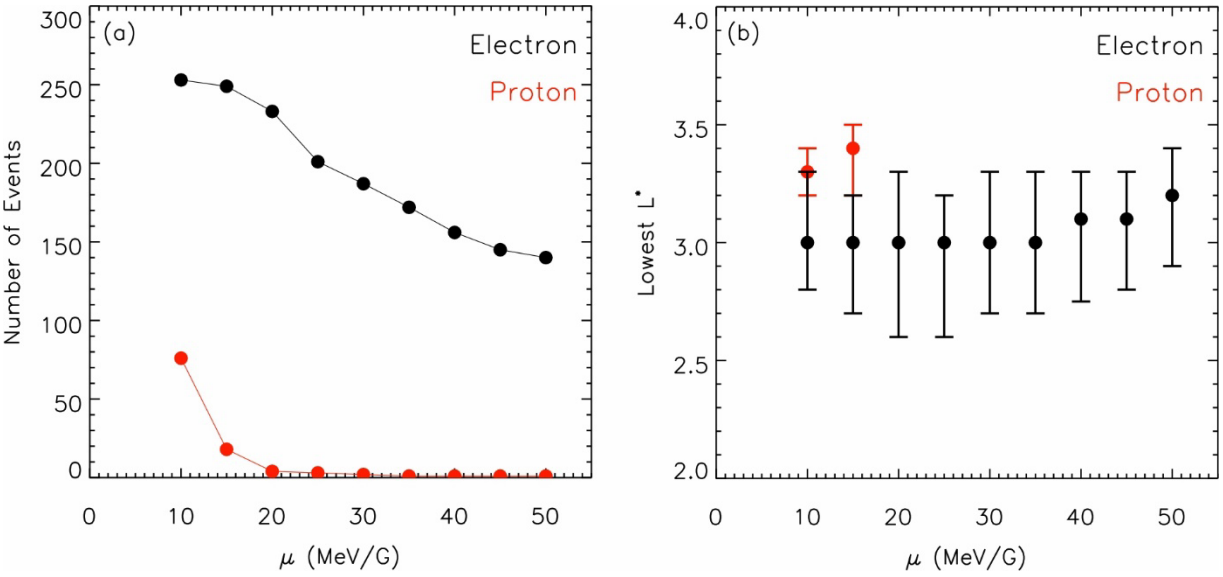

Figure 3. (a) Number of deep penetration events of electrons (in black) and protons (in red) with K=0.14 $G^{1/2}Re$ as a function of μ from 15 March 2013 to 16 July 2019, and (b) the corresponding penetration depth, with the dots showing the medians and the bars showing the range between 25th and 75th percentiles.

We also conducted a statistical analysis of the penetration depth of the deep penetration events. Figure 3(b) shows the statistics on the lowest L^* of these deep penetrations of electrons and protons, i.e., the lowest L^* that daily-averaged PSD enhanced by at least a factor of 2. The dots show the medians, and the bars show the ranges between the lower and upper quartiles. The penetration depth is not shown for protons with μ≥20 MeV/G due to low statistics. Figure 3(b) shows that electrons often penetrate deeper than protons: about half of electron deep

196 penetration events occurred at $L^* \lesssim 3$, most of which occurred at $L^* \lesssim 3.3$, while the majority of
197 proton deep penetrations stayed above $L^* \sim 3.2$.

198 Figure 3 quantitatively demonstrates the systematic differences in the occurrence
199 frequency, penetration depth, and energy dependence of deep penetration of electrons and
200 protons: energetic electrons penetrate to low L-shells much more frequently and deeply than
201 protons, and lower-energy particles penetrate to lower L-shells more easily than higher-energy
202 particles.

203

204 2.3 Timescales of Energetic Electron and Proton Deep Penetration Using Dual-Probe
205 Observations

206 In the previous subsection, daily-averaged PSDs were used to explore the occurrence
207 frequency and depth of energetic electron and proton deep penetration. However, it is worth
208 noting that these deep penetration events can occur in a timescale much faster than one day.
209 For example, Su et al. (2016) showed one fast injection event during which μ=2.5 MeV/G, K=0.3
210 $G^{1/2}Re$ electron flux enhanced significantly at L down to ~2.5 within half a day. Zhao et al.
211 (2017) studied one deep penetration event of energetic electrons during which the electron
212 fluxes were enhanced by orders of magnitude at L~3 – 4 within ~2 hours. In addition, Califf et
213 al. (2022) studied three deep penetration events, each showing an enhancement timescale of
214 electrons on the order of a few hours at L<4. Thus, we also investigate statistically how fast
215 these deep penetration events occur utilizing the PSD data of both Van Allen Probes.

216 The two Van Allen Probes operated in a configuration that followed each other, and the
217 time separation between their orbits ranged from 0 – ~9 hours. This configuration is ideal for
218 studying the timing of deep penetration events. For each identified event, we compare the PSD
219 calculated using both Probes' data pass-by-pass, and the shortest time it takes for PSD to
220 enhance by at least an order of magnitude over a $\Delta L^* > 0.5$ at $L^* < 4$ is recorded. Figure 4 shows an
221 example during a fast, deep penetration event of electrons. The electron phase space densities
222 of a range of μ are shown in this figure, using data from both Van Allen Probes during 10 – 11
223 May 2019. The two highlighted outbound passes show that the electron phase space density
224 increased by a few orders of magnitude at $L^* < 4$ within ~1.8 hours. This example suggests that
225 electron deep penetration can occur faster than a couple of hours.

226 It is worth noting that due to the varying separation between the two Probes, the time
227 calculated here for the deep penetration is only an upper bound: the actual time it takes for
228 electron PSD enhancements is very likely even shorter, which could not be revealed due to
229 limited spatiotemporal coverage of the satellite observations. Also, note that to exclude the
230 potential MLT dependence in the energetic particle deep penetration (e.g., Zhao et al., 2017),
231 the inbound (outbound) passes are compared to inbound (outbound) passes only.

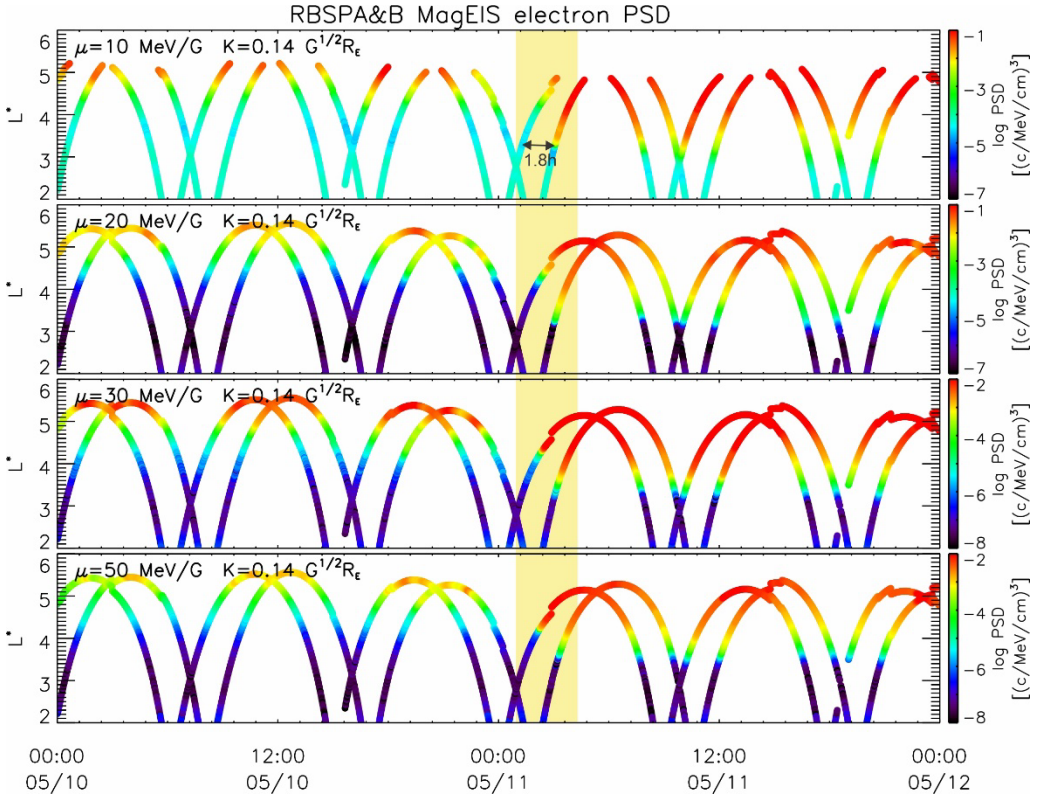

Figure 4. The phase space density of electrons with μ=10, 20, 30, and 50 MeV/G and K=0.14 $G^{1/2}Re$ as a function of L^* and time, from 10 – 11 May 2019, using data from both Van Allen Probes.

Applying the same technique to the deep penetration events identified in Section 2.2 (during which the daily-averaged PSD increased by at least a factor of 2 within a day over $\Delta L^* \geq 0.5$ at $L^* < 4$), the time it takes for each event to occur is calculated, and statistical results are shown in Figure 5. The calculation is only performed for events during which both probes provided good L-shell coverage (PSD data are available at L^* down to at least 3). These include most electron deep penetration events in the Van Allen Probes era and most proton deep penetration events after 2016. Each panel of Figure 5 shows, for a specific population, the numbers and corresponding percentages of deep penetration events which occurred within 0 – 3 hours, 3 – 6 hours, 6 hours – an orbital period of the Van Allen Probes (~9 hours), or more than an orbital period, using both Probes' PSD data. Note that, based on the statistics over 7 years and a half, the time separation of the two Van Allen Probes evenly distributed over the bins of 0 – 3 hours (~33%), 3 – 6 hours (~34%), and 6 – ~9 hours (~33%). However, it is statistically more likely for deep penetration events to occur between passes with a longer time separation due to a longer time window.

Overall, Figure 5 (a-c) shows that the majority of electron deep penetration events occurred on a timescale of several hours. For μ=10 MeV/G, K=0.14 $G^{1/2}Re$ electrons, 71.3% of events occurred within an orbital period of the Van Allen Probes (~9 hours), and 12.6% even occurred

within 3 hours. As μ increases, the deep penetration event takes slightly longer to occur. However, even for μ=50 MeV/G, K=0.14 $G^{1/2}$Re electrons, most events (66.3%) still occurred within ~9 hours, and 7.9% occurred within 3 hours. These results suggest very fast, deep penetrations of energetic electrons to low L-shells in a statistical sense, especially considering that the time calculated here is an upper bound due to limited spatiotemporal coverage. Such fast, deep penetrations are not likely caused by inward radial diffusion, which in general occurs on a timescale of many drift periods of electrons (the drift period of 10s-100s of keV electrons at L<4 is on the order of hours) (e.g., Zhao and Li, 2013). Other mechanisms, such as non-diffusive radial transport caused by enhanced convection electric field (e.g., Su et al., 2016; Califf et al., 2017) or localized DC electric field (e.g., Zhao et al., 2017; Lejosne et al., 2018; Califf et al., 2022), should be considered.

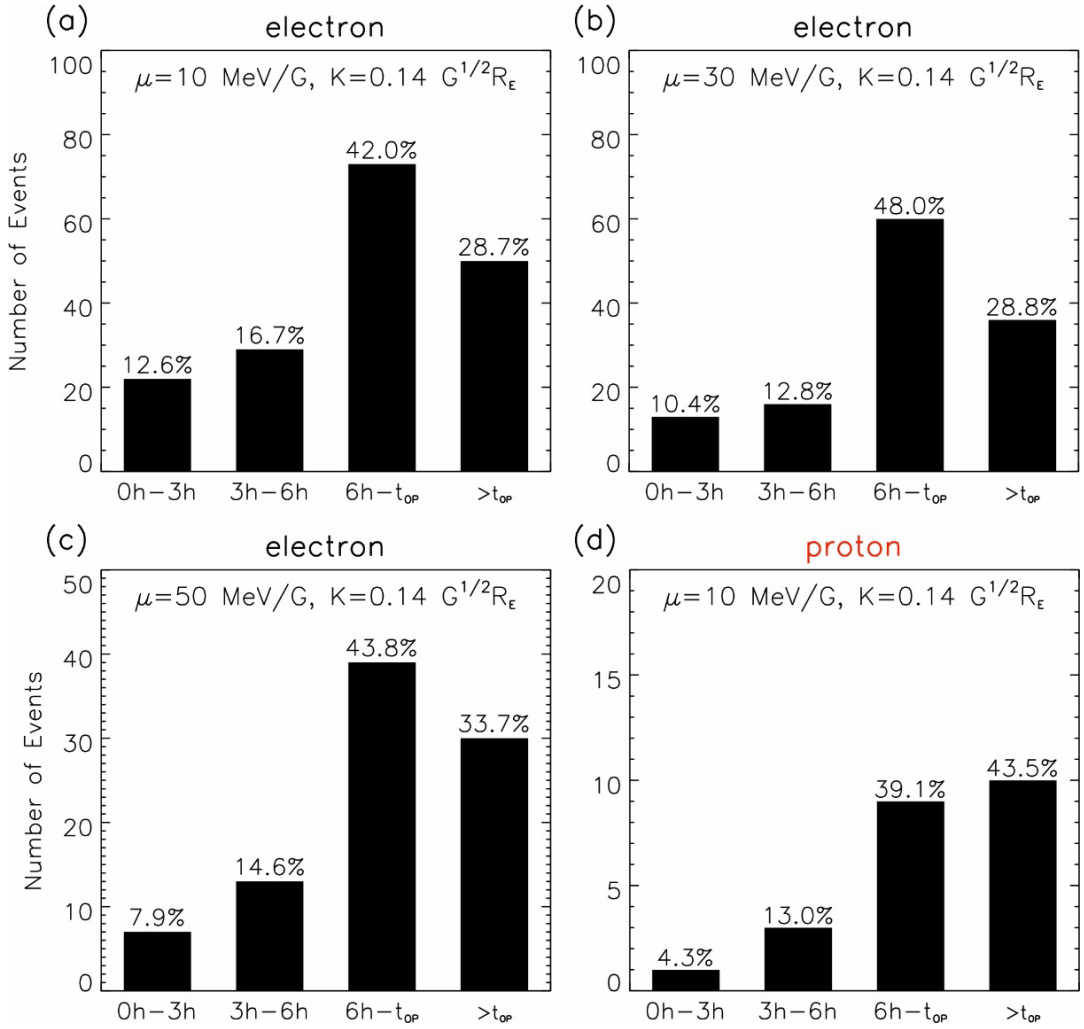

Figure 5. The number and corresponding percentage of deep penetration events that occurred within 0-3h, 3-6h, 6h-t_{OP} (satellite orbital period, ~9h), and >t_{OP}, using data from both Van Allen Probes from 15 March 2013 to 16 July 2019, for (a-c) μ=10, 30, and 50 MeV/G, K=0.14 $G^{1/2}$Re electrons and (d) μ=10 MeV/G, K=0.14 $G^{1/2}$Re protons.

On the other hand, the proton deep penetration events occurred relatively slowly compared to those of electrons. Figure 5(d) shows that, for μ=10 MeV/G, K=0.14 $G^{1/2}$Re protons, 56.5% of events occurred within an orbital period, and only 4.3% (1 event) occurred within 3 hours. For μ=15 MeV/G, K=0.14 $G^{1/2}$Re protons, no deep penetration event occurred within 6 hours, and only 2 events (20%) occurred within ~9 hours. For protons with higher μ values, no event occurred within an orbital period, though the statistics are poor due to the very limited number of events. These results suggest that protons penetrate to low L-shells at a slower pace compared to electrons with similar μ and K.

2.4 Differences in Electron and Proton Phase Space Density Radial Gradient

We have shown systematic differences in electron and proton deep penetrations: energetic electrons penetrate to low L-shells more frequently, deeply, and faster than protons with similar energies. It is thus of great interest to find out which mechanisms are responsible for such differential behaviors of charged particles of different species. A superposed epoch analysis of electron and proton PSD radial profiles is conducted to tackle this problem. Figure 6 shows the statistics of daily-averaged PSD radial profiles for electrons (top panels) and protons (bottom panels) one day before deep penetration events of electrons with the corresponding μ and K. We focus on electron deep penetration events since all proton deep penetration events identified in this study were accompanied by deep penetration of electrons with same μ and K. Note that most electron deep penetration events were not accompanied by proton deep penetration. For instance, μ=10 MeV/G, K=0.14 $G^{1/2}$Re proton deep penetration was only observed in ~30% of deep penetration of electrons with the same μ and K, and for μ=20 – 50 MeV/G particles, this number decreased to a few percent. In Figure 6, each grey curve shows the PSD radial profile during one event, the red curve shows the median of the grey curves, and the black curves show the lower and upper quartiles.

Systematic differences can be observed in PSD radial gradients of electrons and protons prior to the electron deep penetration events. Statistically, prior to the electron deep penetration events, electrons have steeper PSD radial gradients than protons with similar μ and K values. The differences become significantly larger as μ increases: μ=20 – 50 MeV/G, K=0.14 $G^{1/2}$Re protons have much shallower PSD radial gradients at L^*~3-5 compared to electrons of the same μ and K. These differences correlate well with the differences in frequency, depth, and timescale of the electron and proton deep penetration.

Figure 7 shows the evolution of the median of the electron PSD radial profile from the superposed epoch analysis results, from 2 days before the electron deep penetration events to 5 days after those. It shows that, statistically, as the deep penetration event occurs, the electron PSD significantly enhances down to L^*~3, creating an even steeper radial gradient down to lower L-shells. This again suggests that most electron deep penetration events are not likely caused by radial diffusion, which often smooths out the radial gradient in PSD. Non-

diffusive radial transport caused by time-varying convection or localized DC electric fields remains the most likely mechanism causing the electron deep penetrations.

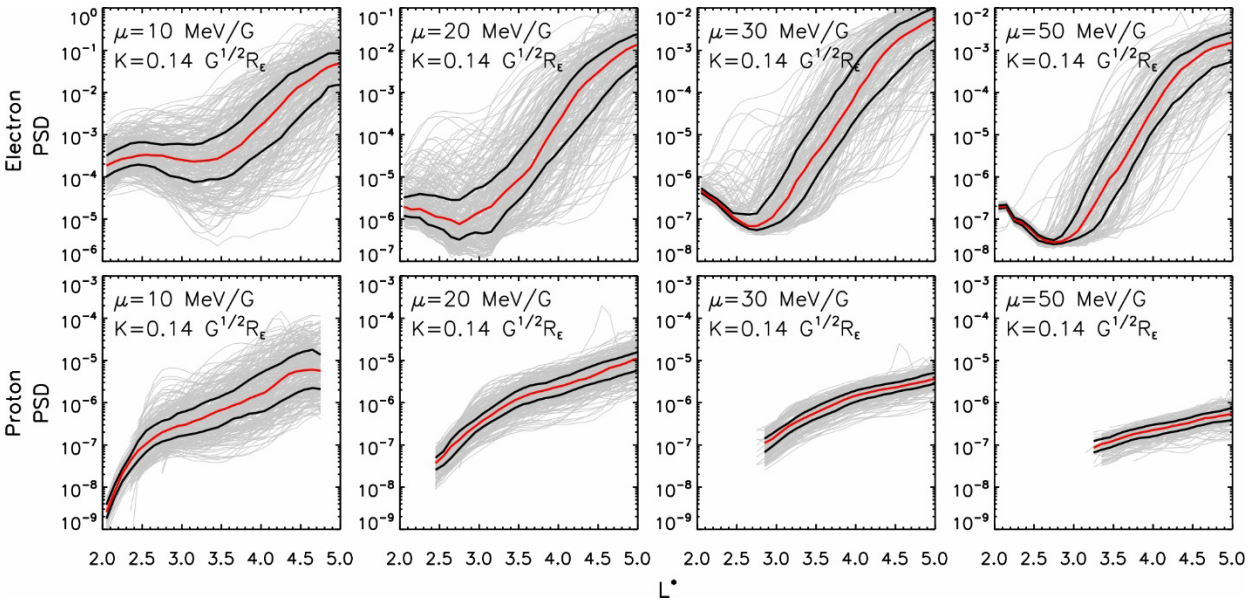

Figure 6. Statistics on daily-averaged phase space density radial profiles of (top) electrons and (bottom) protons with μ=10, 20, 30, and 50 MeV/G and K=0.14 $G^{1/2}$Re, one day before the deep penetration events of electrons with the corresponding μ and K. In each panel, the grey lines show PSD data for deep penetration events, the red line shows the median of the grey lines, and the black lines show the 25th and 75th percentiles.

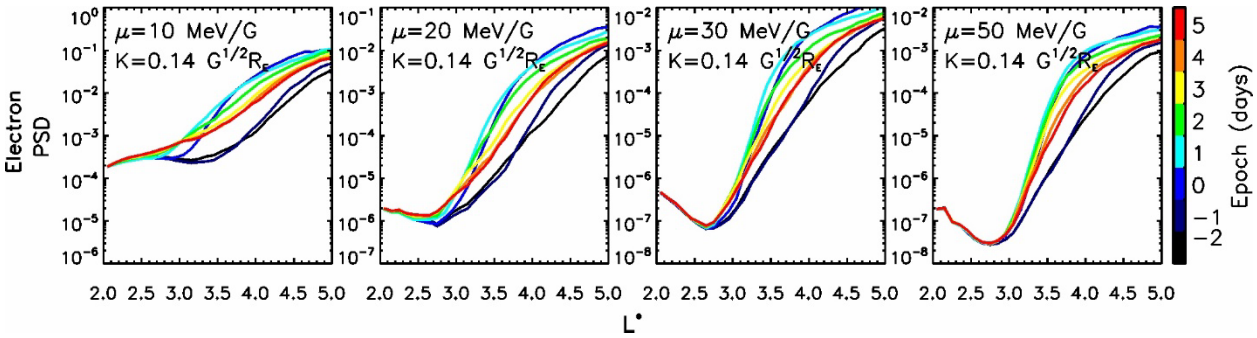

Figure 7. Superposed epoch analysis results on the evolution of daily-averaged phase space density radial profiles (median) of electrons with μ=10, 20, 30, and 50 MeV/G and K=0.14 $G^{1/2}$Re, from 2 days before the deep penetration events to 5 days after those.

Though the role of non-diffusive radial transport on electron deep penetration is very important, the very fast, deep penetration events shown in this study are not likely due to

electrons' direct access from the plasma sheet. For example, if a 100 keV electron gains 100 keV within a drift orbit by convection electric field (which corresponds to a polar cap potential drop greater than 100 kV and thus very strong convection), it would only move from L~4 to L~3.2 in a dipole field. Thus, it is very likely that these fast electron PSD enhancements at low L-shells are due to the inward radial transport of electrons that pre-exist in the inner magnetosphere. A positive PSD radial gradient is needed to enhance the particle PSD at low L-shells by this mechanism. A larger radial gradient suggests that more particles at higher L-shells are available and can be readily transported earthward. With a shallower PSD radial gradient, the inward movement can still be present, but the enhancement at low L-shells would be less significant. Thus, different PSD radial gradients of electrons and protons can be a crucial factor contributing to the differential deep penetration of the two species.

3. Discussion and Conclusion

This statistical study shows the systematic differences in energetic electron and proton deep penetration to L<4 in terms of penetration frequency, depth, and timescale, and suggests that the PSD radial gradient is a vital factor in causing such differential behaviors. It is thus of great interest to know what caused such differences in PSD radial gradients of energetic electrons and protons in the first place.

A positive PSD radial gradient usually requires particle sources at high L-shells and sinks at low L-shells. The large-scale convection electric field is a well-known source process that brings plasma sheet electrons and protons earthward and contributes to the positive radial gradient in PSD (e.g., Korth et al., 1999). However, if the large-scale convection electric field is symmetric at dawn and dusk, electrons and protons with similar energies should have access to similar L-shells (e.g., Korth et al., 1999; Zhao et al., 2017; Lejosne et al., 2018; Califf et al., 2022). In addition, in the plasma sheet, the average temperature of protons is ~5 – 10 times higher than electrons (e.g., Baumjohann, 1993). So, more abundant energetic protons at high L-shells, and thus steeper PSD radial gradients, would actually be expected if the convection electric field is the only driver.

Instead, this steeper radial gradient in electron PSD could be related to more efficient loss of electrons in the slot region than protons with similar energies in the range of 100s of keV. Energetic electrons in the slot region are subject to nearly continuous scattering loss caused by plasmaspheric hiss waves, VLF transmitter waves, lightning-generated whistler waves, and others (e.g., Abel and Thorne, 1998; Claudepierre et al., 2020; Xiang et al., 2020). In contrast, the loss of 100s of keV protons at L~3 – 4 is mainly caused by charge exchange processes, which is often less efficient than electron loss at this region. For example, using Van Allen Probes observations, Claudepierre et al. (2020) showed that the empirical lifetime of 300 keV electrons at L=3 (corresponding to μ~20 – 30 MeV/G) is about 2 days. In comparison, the lifetime of 300 keV protons at L=3 by charge exchange loss is on the order of 10s – 100 days (e.g., Ebihara and

Ejiri, 2003; Illie et al., 2012). Thus, more efficient loss of energetic electrons at L~3 – 4 could be an important factor that leads to a steeper radial gradient in electron PSD.

In addition, some mechanisms that act differently on energetic electrons and protons may also contribute to their differential behaviors. One such mechanism is the DC electric field driven by the Subauroral Polarization Streams (SAPS). SAPS are fast westward ionospheric ion drifts at subauroral latitudes. It corresponds to a poleward electric field in the ionosphere and a radial electric field in the magnetosphere, mainly in the dusk and midnight sectors. Due to its dawn-dusk asymmetry, SAPS has been shown to affect protons and electrons differently and is potentially able to inject electrons deeper than protons (e.g., Lejosne et al., 2018; Califf et al., 2022). Combined with a steeper radial gradient in PSD, the differential effect of SAPS on electrons and protons could be further enhanced.

It is also worth noting that positive feedback could be established for electron deep penetration. As shown in Figure 7, deep penetration events often create a steeper PSD radial gradient down to even lower L-shells. With a steeper PSD radial gradient at lower L, inward radial transport would become more efficient, and more frequent and deeper penetrations would be further observed.

In summary, using multi-year PSD data from Van Allen Probes, this study quantitatively demonstrates systematic differences in electron and proton deep penetration: energetic electron deep penetration to low L-shells occurs more frequently, deeply, and faster than proton deep penetration. Such differential deep penetration can be explained by the steeper PSD radial gradient of electrons than protons, which could be partly due to the faster loss of electrons in the slot region, though other mechanisms could also play a role. Future modeling work is needed to fully understand the underlying mechanisms of differential behaviors of electron and proton deep penetration.

Acknowledgment

This research was supported by the NSF Grant AGS 2140934 and NASA Grant 80NSSC22K0356. We acknowledge Van Allen Probes RBSP-ECT and RBSPICE instrument teams for the use of their data.

Data Availability Statement

Van Allen Probes MagEIS data used in this paper are publicly available at https://rbsp-ect.newmexicoconsortium.org/science/DataDirectories.php. RBSPICE data are publicly available at http://rbspice.ftecs.com. The Dst index is available at http://omniweb.gsfc.nasa.gov.

References

Abel, B., and R. M. Thorne (1998), Electron scattering loss in Earth's inner magnetosphere: 1. Dominant physical processes, J. Geophys. Res., 103(A2), 2385–2396.

Baumjohann, W. (1993). The near-Earth plasma sheet: An AMPTE/IRM perspective, Space Sci. Rev., 64, 141–163.

Blake, J. B., Kolasinski, W. A., Fillius, R. W., & Mullen, E. G. (1992). Injection of electrons and protons with energies of tens of MeV into L < 3 on 24 March 1991. Geophysical Research Letters, 19(8), 821–824. https://doi.org/10.1029/92GL00624.

Blake, J. B., Carranza, P. A., Claudepierre, S. G., Clemmons, J. H., Crain, Jr, W. R., Dotan, W. R., et al. (2013). The magnetic electron ion spectrometer (MagEIS) instruments aboard the radiation belt storm probes (RBSP) spacecraft. Space Science Reviews, 179, 383–421. https://doi.org/10.1007/s11214-013-9991-8.

Califf, S., Li, X., Wolf, R. A., Zhao, H., Jaynes, A. N., Wilder, F. D., … Redmon, R. (2016). Large-amplitude electric fields in the inner magnetosphere: Van Allen Probes observations of subauroral polarization streams. Journal of Geophysical Research: Space Physics, 121, 5294–5306. https://doi.org/10.1002/2015JA022252.

Califf, S., Li, X., Zhao, H., Kellerman, A., Sarris, T. E., Jaynes, A., & Malaspina, D. M. (2017). The role of the convection electric field in filling the slot region between the inner and outer radiation belts. Journal of Geophysical Research: Space Physics, 122, 2051–2068. https://doi.org/10.1002/2016JA023657.

Califf, S., Zhao, H., Gkioulidou, M., Manweiler, J. W., Mitchell, D. G., & Tian, S. (2022). Multi-event study on the connection between subauroral polarization streams and deep energetic particle injections in the inner magnetosphere. Journal of Geophysical Research: Space Physics, 127, e2021JA029895. https://doi.org/10.1029/2021JA029895.

Claudepierre, S. G., O'Brien, T. P., Fennell, J. F., Blake, J. B., Clemmons, J. H., Looper, M. D., … Spence, H. E. (2017). The hidden dynamics of relativistic electrons (0.7–1.5 MeV) in the inner zone and slot region. Journal of Geophysical Research: Space Physics, 122, 3127–3144. https://doi.org/10.1002/2016JA023719.

Claudepierre, S. G., Ma, Q., Bortnik, J., O'Brien, T. P., Fennell, J. F., & Blake, J. B. (2020). Empirically estimated electron lifetimes in the Earth's radiation belts: Van Allen Probe observations. Geophysical Research Letters, 47, e2019GL086053. https://doi.org/10.1029/2019GL086053.

Claudepierre, S. G., Blake, J. B., Boyd, A. J., Clemmons, J. H., Fennell, J. F., Gabrielse, C., et al. (2021). The magnetic electron ion spectrometer: A review of on-orbit sensor performance, data, operations, and science. Space Science Reviews, 217, 80. https://doi.org/10.1007/s11214-021-00855-2.

Ebihara, Y., and M. Ejiri (2003), Numerical simulation of the ring current: Review, Space Sci. Rev., 105(1-2), 377–452.

Frank, L. A. (1967), On the extraterrestrial ring current during geomagnetic storms, J. Geophys. Res., 72(15), 3753–3767, doi:10.1029/JZ072i015p03753.

Gkioulidou, M., A. Y. Ukhorskiy, D. G.Mitchell, and L. J. Lanzerotti (2016), Storm time dynamics of ring current protons: Implications for the long-term energy budget in the inner magnetosphere, Geophys. Res. Lett., 43, 4736–4744, doi:10.1002/2016GL068013.

Ilie, R., R. Skoug, H. Funsten, M. Liemohn, J. Bailey, and M. Gruntman (2012), The impact of geocoronal density on ring current development, J. Atmos. Sol. Terr. Phys., 99, 92–103, doi:10.1016/j.jastp.2012.03.010.

Khoo, L.-Y., Li, X., Zhao, H., Thaller, S. A., & Hogan, B. (2021). Multievent studies of sudden energetic electron enhancements in the inner magnetosphere and its association with plasmapause positions. Journal of Geophysical Research: Space Physics, 126, e2021JA029769. https://doi.org/10.1029/2021JA029769.

Korth, H., Thomsen, M. F., Borovsky, J. E., & McComas, D. J. (1999). Plasma sheet access to geosynchronous orbit. Journal of Geophysical Research, 104(A11), 25,047–25,061. https://doi.org/10.1029/1999JA900292.

Krimigis, S. M., G. Gloeclker, R. W. McEntire, T. A. Potemra, F. L. Scarf, and E. G. Shelley (1985), The magnetic storm of September 4, 1984, a synthesis of ring current spectra and energy densities measured with AMPTE/CCE, Geophys. Res. Lett., 12(5), 329–332, doi:10.1029/GL012i005p00329.

Li, X., Roth, I., Temerin, M., Wygant, J. R., Hudson, M. K., & Blake, J. B. (1993). Simulation of the prompt energization and transport of radiation belt particles during the March 24, 1991 SSC. Geophysical Research Letters, 20(22), 2423–2426. https://doi.org/10.1029/93GL02701.

Li, X., Baker, D. N., Zhao, H., Zhang, K., Jaynes, A. N., Schiller, Q., … Temerin, M. (2017). Radiation belt electron dynamics at low L (<4): Van Allen Probes era versus previous two solar cycles. Journal of Geophysical Research: Space Physics, 122, 5224–5234. https://doi.org/10.1002/2017JA023924.

Lyons, L. R., & Thorne, R. M. (1973). Equilibrium structure of radiation belt electrons. Journal of Geophysical Research, 78(13), 2142–2149. https://doi.org/10.1029/JA078i013p02142.

Mauk, B. H., Fox, N. J., Kanekal, S. G., Kessel, R. L., Sibeck, D. G., & Ukhorskiy, A. (2012). Science objectives and rationale for the radiation belt storm probes mission. Space Science Reviews, 179, 1–15. https://doi.org/10.1007/s11214-012-9908-y10.1007/978-1-4899-7433-4_2.

Mitchell, D. G., Lanzerotti, L. J., Kim, C. K., Stokes, M., Ho, G., Cooper, S., … Kerem, S. (2013). Radiation belt storm probes ion composition experiment (RBSPICE). Space Science Reviews, 179, 263–308. https://doi.org/10.1007/s11214-013-9965-x.

Reeves, G. D., Friedel, R. H. W., Larsen, B. A., Skoug, R. M., Funsten, H. O., Claudepierre, S. G.,…Baker, D. N. (2016). Energy-dependent dynamics of keV to MeV electrons in the inner zone, outer zone, and slot regions. Journal of Geophysical Research: Space Physics, 121, 397–412. https://doi.org/10.1002/2015JA021569.

Ripoll, J.-F., Reeves, G. D., Cunningham, G. S., Loridan, V., Denton, M., Santolík, O., … Ukhorskiy, A. Y. (2016). Reproducing the observed energy-dependent structure of Earth's electron radiation belts during storm recovery with an event-specific diffusion model. Geophysical Research Letters, 43, 5616–5625. https://doi.org/10.1002/2016GL068869.

Sarris, T. E., & Li, X. (2016). Calculating ultra-low-frequency wave power of the compressional magnetic field vs. L and time: Multi-spacecraft analysis using the Van Allen Probes, THEMIS and GOES.Annales Geophysicae, 34, 565–571. https://doi.org/10.5194/angeo-34-565-2016.

Schiller, Q., Kanekal, S. G., Jian, L. K., Li, X., Jones, A., Baker, D. N., et al. (2016). Prompt injections of highly relativistic electrons induced by interplanetary shocks: A statistical study of Van Allen Probes observations. Geophysical Research Letters, 43(12), 12317–12324. https://doi.org/10.1002/2016GL071628.

Smith, P. H., and R. A. Hoffman (1973), Ring current particle distributions during the magnetic storms of December 16–18, 1971, J. Geophys. Res., 78(22), 4731–4737, doi:10.1029/JA078i022p04731.

Stern, D. P. (1973). A study of the electric field in an openmagnetospheric model. Journal of Geophysical Research, 78(31), 7292–7305. https://doi.org/10.1029/JA078i031p07292.

Su, Y.-J., Selesnick, R. S., & Blake, J. B. (2016). Formation of the inner electron radiation belt by enhanced large-scale electric fields. Journal of Geophysical Research: Space Physics, 121, 8508–8522. https://doi.org/10.1002/2016JA022881.

Tsyganenko, N. A. (1989). A magnetospheric magnetic field model with a warped tail current sheet. Planetary and Space Science, 37(1), 5–20. https://doi.org/10.1016/0032-0633(89)90066-4.

Turner, D. L., Claudepierre, S. G., Fennell, J. F., O'Brien, T. P., Blake, J. B., Lemon, C., … Angelopoulos, V. (2015). Energetic electron injections deep into the inner magnetosphere associated with substorm activity. Geophysical Research Letters, 42, 2079–2087. https://doi.org/10.1002/2015GL063225.

Turner, D. L., et al. (2016), Investigating the source of near-relativistic and relativistic electrons in Earth's inner radiation belt, J. Geophys. Res. Space Physics, 122, 695–710, doi:10.1002/2016JA023600.

503 Volland, H. (1973). A semiempirical model of large-scale magnetospheric electric fields. Journal
504 of Geophysical Research, 78(1), 171–180. https://doi.org/10.1029/JA078i001p00171.

505 Williams, D. J. (1981), Ring current composition and sources: An update, Planet. Space Sci., 29,
506 1195–1203.

507 Xiang, Z., Li, X., Ni, B., Temerin, M. A., Zhao, H., Zhang, K., & Khoo, L.Y. (2020). Dynamics of
508 energetic electrons in the slot region during geomagnetically quiet times: Losses due to
509 wave-particle interactions versus source from cosmic ray albedo neutron decay (CRAND).
510 Journal of Geophysical Research: SpacePhysics, 125, e2020JA028042. https://doi.org/
511 10.1029/2020JA028042.

512 Zhao, H., & Li, X. (2013). Modeling energetic electron penetration into the slot region and inner
513 radiation belt. Journal of Geophysical Research: Space Physics, 118, 6936–6945.
514 https://doi.org/10.1002/2013JA019240.

515 Zhao, H., Li, X., Baker, D. N., Fennell, J. F., Blake, J. B., Larsen, B. A.,…Rodriguez, J. V. (2015). The
516 evolution of ring current ion energy density and energy content during geomagnetic storms
517 based on Van Allen Probes measurements. Journal of Geophysical Research: Space Physics, 120,
518 7493–7511. https://doi.org/10.1002/2015JA021533.

519 Zhao, H., et al. (2016), Ring current electron dynamics during geomagnetic storms based on the
520 Van Allen Probes measurements, J. Geophys. Res. Space Physics, 121, 3333–3346,
521 doi:10.1002/2016JA022358.

522 Zhao, H., D. N. Baker, S. Califf, X. Li, A. N. Jaynes, T. Leonard, S. G. Kanekal, J. B. Blake, J. F.
523 Fennell, S. G. Claudepierre, D. L. Turner, G. D. Reeves, and H. E. Spence (2017). Van Allen Probes
524 measurements of energetic particle deep penetration into the low L region (L<4) during the
525 storm on 8 April 2016, J. Geophys. Res. Space Physics, 122.
526 https://doi.org/10.1002/2017JA024558.